Philosophical Magazine

ISSN: 1478-6435 (Print) 1478-6443 (Online) Journal homepage: http://www.tandfonline.com/loi/tphm20

n-type conductivity in Si-doped amorphous AlN: an ab initio investigation

Murat Durandurdu

To cite this article: Murat Durandurdu (2016): n-type conductivity in Si-doped amorphous AlN: an ab initio investigation, Philosophical Magazine, DOI: 10.1080/14786435.2016.1155783

To link to this article: http://dx.doi.org/10.1080/14786435.2016.1155783

Published online: 11 Mar 2016.

PHILOSOPHICAL MAGAZINE, 2016
http://dx.doi.org/10.1080/14786435.2016.1155783

Taylor & Francis
Taylor & Francis Group

n-type conductivity in Si-doped amorphous AlN: an *ab initio* investigation

Murat Durandurdu

Department of Materials Science & Nanotechnology Engineering, Abdullah Gül University, Kayseri, Turkey

ABSTRACT

We report the electronic structure and topology of a heavily Si-doped amorphous aluminium nitride ($Al_{37.5}Si_{12.5}N_{50}$) using *ab initio* simulations. The amorphous $Al_{37.5}Si_{12.5}N_{50}$ system is found to be structurally similar to pure amorphous aluminium nitride. It has an average coordination number of about 3.9 and exhibits a small amount of Si–Si homopolar bonds. The formation of Si–Al bonds is not very favourable. ElTPHMectronic structure calculations reveal that the Si doping has a negligible effect on the band gap width but causes delocalization of the valence band tail states and a shift of the Fermi level towards the conduction band. Thus, amorphous $Al_{37.5}Si_{12.5}N_{50}$ alloys show n-type conductivity.

ARTICLE HISTORY
Received 9 November 2015
Accepted 15 February 2016

KEYWORDS
Ab initio method; amorphous semiconductors; density-functional method; electrical conductivity; aluminium alloys; molecular dynamic simulations

1. Introduction

Aluminium nitride (AlN) is a well-known ceramic and has high technological relevance because of its outstanding optical, dielectric and mechanical properties such as high-temperature stability, high thermal conductivity, good dielectric strength, high hardness, deep ultraviolet transparency, etc. [1–19]. All these properties make AlN a unique material having a wide range of refractory, high-temperature electronics, microelectronic, optoelectronic and micromechanical applications [1–19].

AlN has three crystalline structures under ambient and high-pressure conditions. The ground state phase of AlN is the hexagonal wurtzite (WZ) structure belonging to the $P6_3mc$ space group [20]. The zinc-blende (ZB) type of AlN within $F\bar{4}3m$ symmetry is the metastable phase of AlN and can be grown as a thin film under some certain circumstances [21]. The rocksalt phase (RS), with the space group of $Fm\bar{3}m$, forms under compression and is quenchable to atmospheric pressure [22]. Another state of AlN is its amorphous form (*a*-AlN), which can easily be prepared using various experimental procedures [23–26]. This form is anticipated to have some important high-tech applications similar to the crystalline phase but it has not been extensively studied as yet.

There have been significant research efforts to improve/control the properties of the crystalline AlN or promote the development of its new technological applications. Doping

CONTACT Murat Durandurdu murat.durandurdu@agu.edu.tr

the hexagonal phase with different elements, such as Mg, Cr, Si, RE, C, etc., leads to various appealing physical phenomena [27–48]. However, some of these have not been scientifically understood yet. The doping *a*-AlN with rare earth elements can provoke some interesting phenomena too and doped *a*-AlN seems to offer some practical applications for optical, photonic and electronic devices [49–54].

Among these dopants, the influence of Si doping on the properties of the WZ crystal has been comprehensively investigated [27–35] because doping drastically changes its electronic structures; in particular, Si-doped WZ-AlN system demonstrates n-type conductivity. Here, one might ask how the Si-doping influences the electronic properties and the microstructure of *a*-AlN. The main objective of the present work is to find an answer to this question. We have generated a heavily Si doped *a*-AlN ($Al_{37.5}Si_{12.5}N_{50}$) model from the liquid state using *ab initio* molecular dynamics (MD) simulations and compared it with a pure *a*-AlN configuration. The $Al_{37.5}Si_{12.5}N_{50}$ amorphous alloy is found to be topologically close to *a*-AlN but it possesses n-type conductivity, similar to the Si-doped WZ-AlN system. Therefore, it is expected that Si-doped *a*-AlN can have some technological applications as well.

2. Computational method

We employed the SIESTA *ab initio* code [55] to generate the amorphous network. The code was successfully applied to study the pressure-induced phase transformation of the WZ-AlN phase [56] and to create a pure *a*-AlN model [57]. In the present work, the simulation parameters of Ref. [57] were adopted. The pseudopotentials followed the Troullier and Martins scheme [58]. The Becke gradient exchange functional [59] and the Lee, Yang, Parr correlation functional [60] were used to compute the exchange correlation energy. The double zeta plus polarized orbitals were chosen as a basis set. For the Brillouin zone integration, only Γ point sampling was used. In order to construct a supercell, a ZB unit cell with eight atoms (four Al atoms four N atoms) was used as a starting structure. One of the Al atoms in the unit cell was substituted by a Si atom and a supercell with 216 atoms (27 Si atoms, 81 Al atoms and 108 N atoms) was generated. The initial supercell was subjected to a high temperature of 5000 K for 1.0 ps, and then, the system was quickly cooled to 3200 K. At this temperature, it was equilibrated for 7.0 ps. The liquid structure was quenched to 300 K in a period of 10 ps. The NPT (constant number of atoms, constant pressure and constant temperature) ensemble was selected to perform the MD simulations. Each time step of the MD simulations was one femtosecond (fs). The velocity rescaling approach was employed to control the temperature. The volume of the supercell at zero pressure was equilibrated using the Parrinello Rahman technique [61] but shear deformations were not allowed. The VESTA program [62] was used to visualize the structure.

3. Results and discussion

Experiments have revealed that the Si concentration has a drastic influence on the atomic structure of the Al–Si–N system. It can exhibit a solid solution, a two-phase composite (nanocomposite), or an amorphous solid solution depending on the Si concentration [63–65]. The solubility limit was reported to be 6 at.% of Si in some studies [63, 64], but a Si concentration of up to 11 at.% yielded a substitutional solid solution in another study [66]. Consequently, there is an uncertainty about the solubility limit at present. In order

to reveal whether the doped amorphous network demonstrates a solid solution or a two-phase composite, its ball-and-stick representation is illustrated in Figure 1. The Si atoms are uniformly distributed in the system, but in some parts of the amorphous network, SiN type structures are dominated, suggesting a two-phase amorphous state.

To have an atomic level picture of the doped amorphous structure and to compare it with the pure *a*-AlN system, first, the partial pair distribution functions (PPDFs) given in

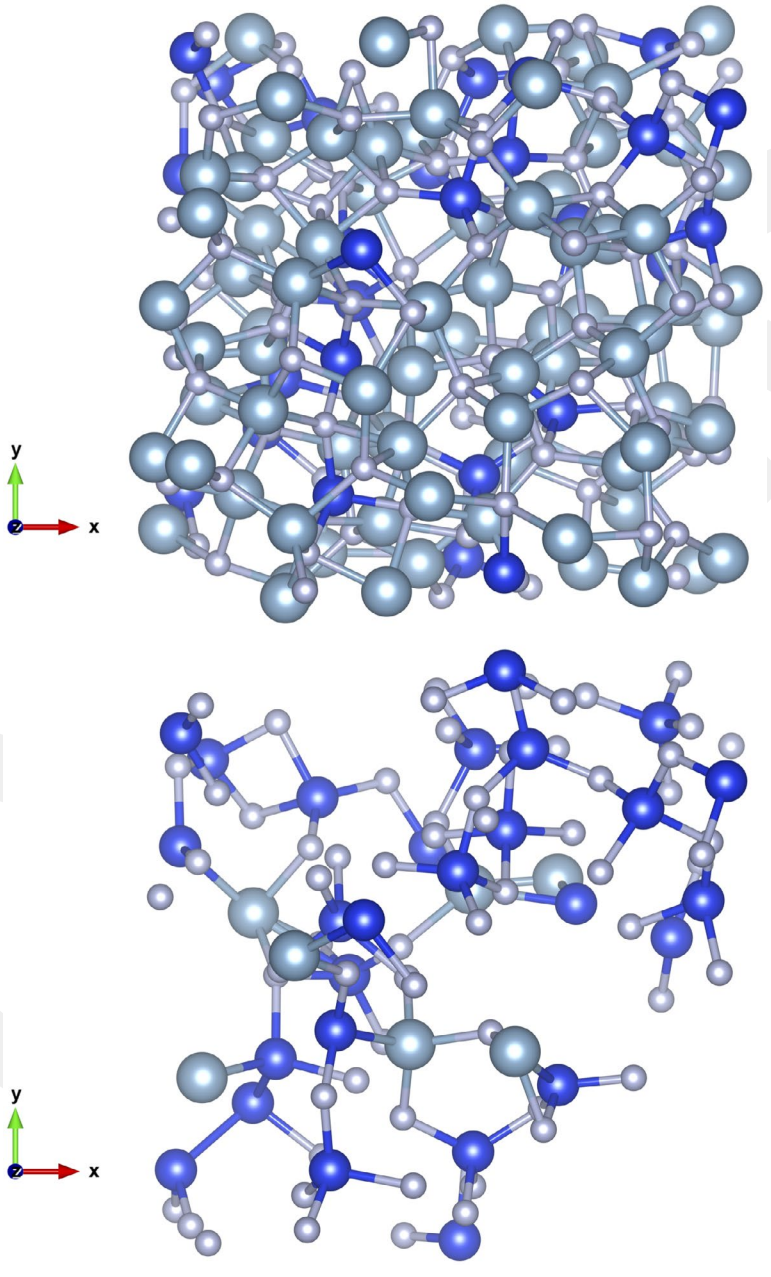

Figure 1. (colour online) The ball-and-stick representation of the $Al_{37.5}Si_{12.5}N_{50}$ model (top) and only Si atoms and their neighbours (bottom) in the model.

Figure 2 are reviewed. The Al–N correlation has the strongest peak at 1.94 Å that is slightly larger than 1.91 Å reported for *a*-AlN [57]. The Al–Al and N–N separations are placed at 3.21 Å and 3.16 Å, respectively. These values are comparable with the Al–Al (3.22 Å) and N–N (3.22 Å) distances formed in *a*-AlN [57]. The shoulders around 2.7–2.90 Å in these correlations are not related to the N–N or Al–Al wrong bonds but arise from edge-sharing units as shown in Figure 3. On the other hand, the peak near 2.33 Å in the Si–Si distribution is a consequence of Si–Si homopolar bonds. In spite of a small amount of Si concentration,

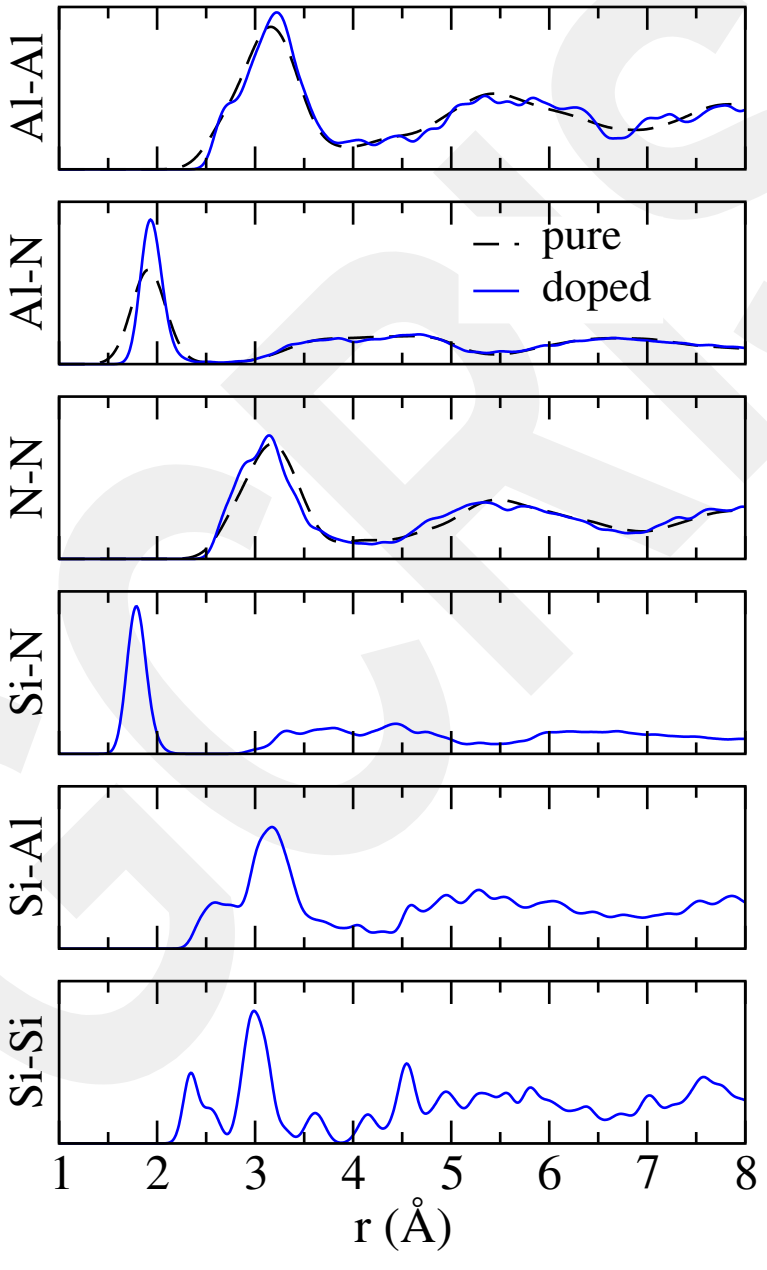

Figure 2. (colour online) Partial pair distribution functions.

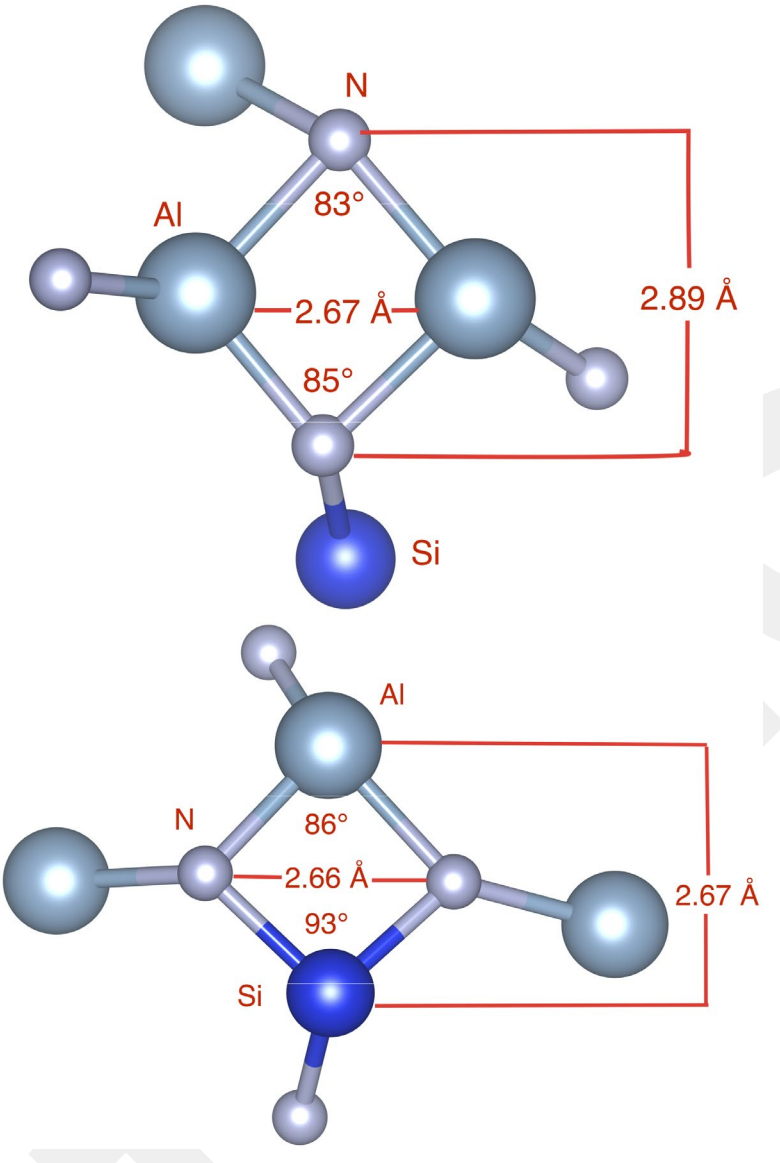

Figure 3. (colour online) Edge sharing configurations (four membered rings).

the strong peak at around 3 Å in the Si–Si correlation reveals that the Si atoms in the model are relatively close to each other, supporting a two-phase amorphous state. The weak peak around 2.6 Å in the Si–Al distribution is also associated with the edge-sharing units as illustrated in Figure 3, but a single Si atom forming bonds with three Al atoms offers a small contribution to this peak as well. The main Si–N peak is located at 1.78 Å, according with the Si–N distance of 1.73 Å [67] or 1.76 Å [68] formed in *a*-Si_2N_3. The PPDFs analysis leads to some important conclusions: (1) The formation of the Si–Al bonds is not very favourable. (2) Neither N nor Al has a tendency to form homopolar bonds, whereas a few Si–Si homopolar bonds exist in the amorphous $Al_{37.5}Si_{12.5}N_{50}$ alloy despite the small amount of Si.

Next, bond-angle distribution (BADF) analysis is carried out to have more knowledge about the local structure. The calculated BADFs are given in Figure 4. The Al–N–Al, N–Al–N, N–Si–N and N–Si–N distributions have two main peaks at around 83°–95° and 105°–113° as seen in *a*-AlN. The strong peak near 105°–113° is linked to the tetrahedral configurations with some distortions, whereas the peak around 83°–95° is associated with the edge-sharing units (see Figure 3). This finding means that the local structure of the amorphous $Al_{37.5}Si_{12.5}N_{50}$ system is somewhat different from the WZ- or ZB-AlN and Si_2N_3 crystals because they do not present edge-sharing units. It should be underlined here that the theoretical studies based on *ab initio* simulations endorse the finding that the formation of the edge-sharing arrangements is a common feature in N-based amorphous materials [69–71]. The threefold-coordinated N atoms produce large angles in the distributions.

In order to describe the short-range order in detail, we additionally estimate the coordination number (CN) using the cut-off distances of 2.47 Å for Al–N, 2.21 Å for Si–N, 2.77 Å for Si–Al and 2.71 Å for Si–Si correlations. The fourfold coordination is dominated for all atoms, i.e. 96% of Si, 84% of Al, 80% of N atoms are tetrahedrally coordinated. The fivefold and threefold configurations are favourable for Al (12%) and N (19%) atoms, respectively. The average CN of the model is 3.9, close to that of *a*-AlN.

A comparison of pure *a*-AlN with the doped samples reveals that Si doping does not significantly affect the short-range order of *a*-AlN since both models are topologically close to each other. Yet, there are two major differences between these two amorphous arrangements. First, the Si-doped amorphous network demonstrates a small amount of chemical disorder, while pure *a*-AlN is chemically ordered. Secondly, the amorphous $Al_{37.5}Si_{12.5}N_{50}$ alloy has no hexagonal (drum-like) nanoclusters unlike *a*-AlN. Subsequently, Si doping somehow inhibits the formation of nanoclusters in the amorphous network.

The influence of Si doping on the electronic structure of *a*-AlN is considered using both the total and the partial density of states (EDOS and PDOS) shown in Figures 5 and 6. For

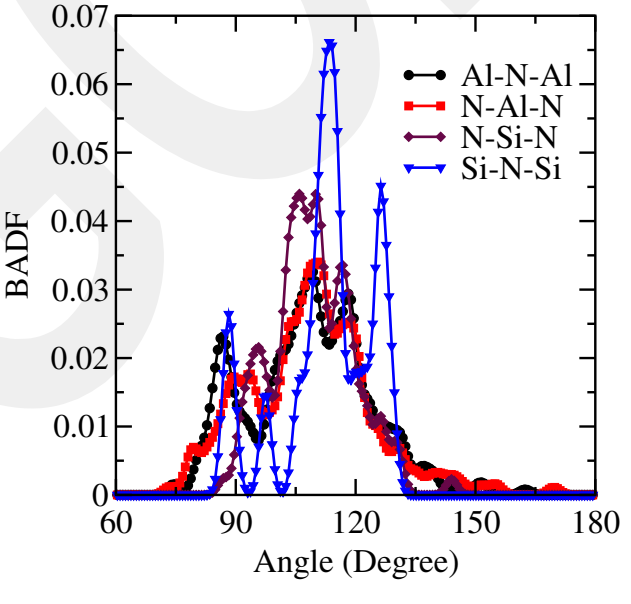

Figure 4. (colour online) The bond angle distribution functions (BADFs).

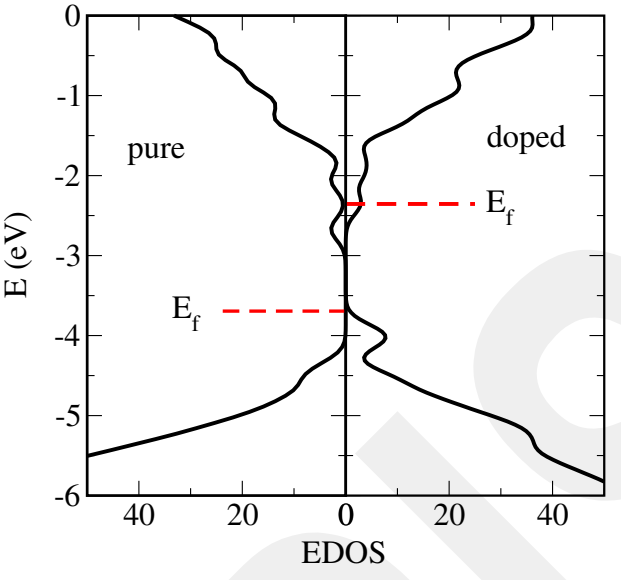

Figure 5. (colour online) Electron density of states (EDOS) for pure and Si-doped *a*-AlN near the band gap region.

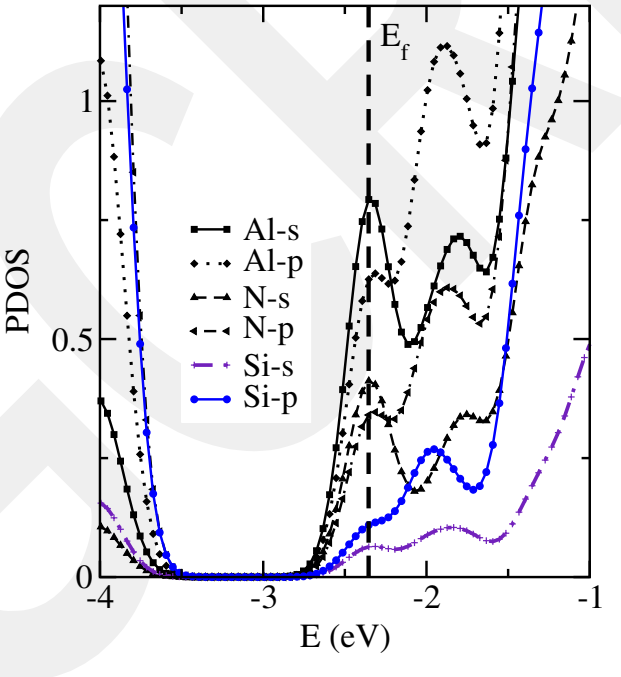

Figure 6. (colour online) Partial density of states near the band gap.

comparison purpose, the EDOS of *a*-AlN is also displayed in Figure 4. The HOMO and LUMO states are located at –4.40434 and –2.67969 eV, respectively, for *a*-AlN, and –3.95845 and –2.35467 eV, respectively, for the amorphous $Al_{37.5}Si_{12.5}N_{50}$ network. As can be inferred from these values and seen clearly from Figure 5, both valance and conduction bands of

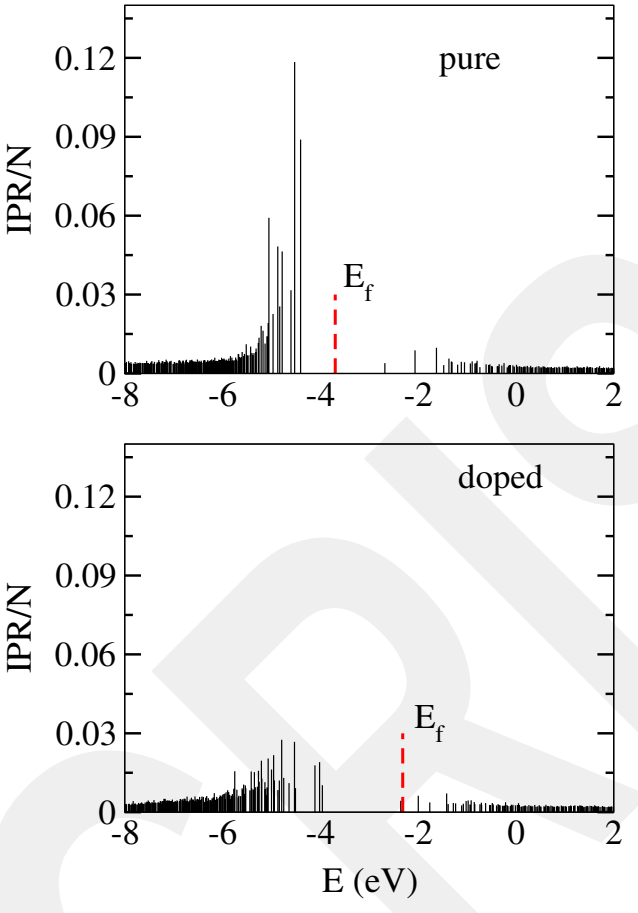

Figure 7. (colour online) IPR of pure and Si-doped *a*-AlN near the band gap region.

the doped material move somewhat to higher energies relative to those of *a*-AlN, but the shift of the valance band is slightly larger than that of the conduction band, resulting in a ~0.1 eV reduction in the band gap energy compared to that of *a*-AlN. On the other hand, doping drastically changes the position of Fermi level from the middle of the band gap towards the conduction band tail, leading to n-type conductivity in the Si-doped *a*-AlN system. This finding is similar to that predicted for the Si-doped WZ-AlN system. In order to determine the contribution of each type of atom to the tail states, we evaluated the PDOS illustrated in Figure 6 and found that the Si atoms provide the lowest contribution to the conduction tail states, while the Al atoms offer the highest one. The upper valance band is derived from the N-p and Si-p states.

To provide additional information about the electronic structure of both pure and doped *a*-AlN and to speculate on the mobility of the electrons in the tail states, we probe the spatial localization of electronic states using the inverse participation ratio (IPR) that is described [72, 73] by $\mathrm{IPR}\left(\psi_j\right) = N\sum_{i=1}^{N} a_i^{j4}/(\sum_{i=1}^{N} a_i^{j2})^2$ where $\psi_i = \sum_{i=1}^{N} a_i^j \phi_i$ is the jth eigenstate. The results are plotted in Figure 7. Each spike in the figure denotes a single electronic eigenvalue. For *a*-AlN, the valence tail states have a rather higher IPR indicating their localization,

whereas the conduction tail states are more extended. This finding is analogous to what has been obtained for *a*-GaN [70]. For the case of the Si-doped amorphous model, we find that not only the conduction tail states but also the valence tail states are quite delocalized, suggesting a possible dopant-induced delocalization and a high mobility in these states.

By following the suggestion of Ref. [70] and using the result of our IPR investigation, we can also propose that p-type doping is anticipated to be more difficult than n-type doping for *a*-AlN since moving the Fermi level to the valence band mobility edge is harder because of the localization of the states.

The present simulation shows that the electronic structure of *a*-AlN can be drastically affected by doping. We did not, however, study the outcome of the dopant concentration on the electronic structure of *a*-AlN. Depending on the Si concentration, its electronic properties might be tunable to desirable values and hence the Si-doped *a*-AlN system could offer some practical applications in technology.

4. Conclusions

The electronic and atomic structures of a heavily Si-doped *a*-AlN ($Al_{37.5}Si_{12.5}N_{50}$) alloy have been determined by means of *ab initio* MD simulations. The Si doping does not have significant impact on the local structure of the amorphous network but it does on its electronic structure. Doping results in delocalization of the valence tail states and a shift of the Fermi level towards the conduction band leading to n-type conductivity in the amorphous $Al_{37.5}Si_{12.5}N_{50}$.

Disclosure statement

No potential conflict of interest was reported by the author.

Funding

This work was supported by the Scientific and Technical Research Council of Turkey (TÜBİTAK) under [grant number 114C100].

References

[1] E.F. McCullen, J.S. Thakur, Y.V. Danylyuk, G.W. Auner, and L.W. Rosenberger, *Investigation of the occupation behavior for oxygen atoms in AlN films using Raman spectroscopy*, J. Appl. Phys. 103 (2008), pp. 063504–063507.
[2] Y. Lee and S. Kang, *Growth of aluminum nitride thin films prepared by plasma-enhanced atomic layer deposition*, Thin Solid Films 446 (2004), pp. 227–231.
[3] F. Jose, R. Ramaseshan, S. Bera, A.K. Tyagi, and B. Raj, *Response of magnetron sputtered AlN films to controlled atmosphere annealing*, J. Phys. D Appl. Phys. 43 (2010), pp. 075305.
[4] A. Artieda, M. Barbieri, C.S. Sandu, and P. Muralt, *Effect of substrate roughness on c-oriented AlN thin films*, J. Appl. Phys. 105 (2009), pp. 024504–024509.
[5] S. Bakalova, A. Szekeres, G. Huhn, K. Havancsak, S. Grigorescu, G. Socol, C. Ristoscu, and I.N. Mihailescu, *Surface morphology of AlN films synthesized by pulsed laser deposition*, Vacuum 84 (2009), pp. 155–157.
[6] H.O. Pierson, *Handbook of Refractory Carbides and Nitrides: Properties, Characteristics Processing and Applications*, Noyes Publications, Westwood, NJ, 1996.

[7] S. Strite and H. Morkoc, *GaN, AlN, and InN: A review*, J. Vac. Sci. Technol. B 10 (1992), pp. 1237–1266.
[8] C. Stampfl and C.G. van de Walle, *Density-functional calculations for III-V nitrides using the local-density approximation and the generalized gradient approximation*, Phys. Rev. B 59 (1998), pp. 5521–5535.
[9] A.W. Weimer, G.A. Cochran, G.A. Eisman, J.P. Henley, B.D. Hook, K.L. Mills, T.A. Guiton, A.K. Knudsen, N.R. Nicholas, J.E. Volmering, and W.G. Moor, *Rapid process for manufacturing aluminum nitride powder*, J. Am. Ceram. Soc. 77 (1994), pp.3–18.
[10] A.V. Virkar, T.B. Jackson, and R.A. Cutler, *Thermodynamic and kinetic effects of oxygen removal on the thermal conductivity of aluminum nitride*, J. Am. Ceram. Soc. 72 (1989), pp. 2031–2042.
[11] T.J. Mroz, *Aluminum nitride*, Ceram. Bull. 71 (1992), pp. 782–784.
[12] Q. Wang, W. Cui, Y. Ge, K. Chen, and Z. Xie, *Preparation of spherical AlN granules directly by carbothermal reduction–nitridation method*, J. Am. Ceram. Soc. 98 (2015), pp. 392–397.
[13] J.H. Edgar, ed., *Properties of Group-III Nitrides, EMIS Data Reviews Series*, IEE, London, 1994.
[14] M.E. Levinshtien, S.L. Rumyantsev, and M.S. Shur, *Properties of Advances Semiconductor Materials : GaN, AIN, InN, BN, SiC, SiGe*, John Wiley and Sons, Inc., New York, 2001.
[15] S.C. Jain, M. Willander, J. Narayan, and R. Van Overstraeten, *III–nitrides: Growth, characterization, and properties*, J. Appl. Phys. 87 (2000), pp. 965–1006.
[16] A. Wilmański, M.M. Bućko, Z. Pędzich, and J. Szczerba, *Salt-assisted SHS synthesis of aluminium nitride powders for refractory applications*, J. Mater. Science and Chem. Eng. 2 (2014), pp. 26–31.
[17] C.M. Lin T.-T. Yen, V.V. Felmetsger, M.A. Hopcroft, J.H. Kuypers, and A.P. Pisano, *Thermally compensated aluminum nitride Lamb wave resonators for high temperature applications*, Appl. Phys. Lett. 97 (2010), pp. 083501–083501.
[18] S. Yin, K.J. Tseng, and J. Zhao, *Design of AlN-based micro-channel heat sink in direct bond copper for power electronics packaging*, Appl. Therm. Eng. 55 (2013), pp. 120–129.
[19] T.M. Tritt (ed.), *Thermal Conductivity: Theory, Properties, and Applications*, Kluwer Academic / Plenum, New York, NY, 2004.
[20] H. Shultz and K.H. Thiemann, *Crystal structure refinement of AlN and GaN*, Solid State Commun. 23 (1977), pp. 815–819.
[21] I.Petrov, E. Mojab, R.C. Powell, J.E. Greene, L. Hultman, and J.E. Sundgren, *Synthesis of metastable epitaxial zinc-blende-structure AlN by solid-state reaction*, Appl. Phys. Lett. 60 (1992), pp. 2491–2493.
[22] Q. Xia, H. Xia, and A.L. Ruoff, *Pressure-induced rocksalt phase of aluminum nitride: A metastable structure at ambient condition*, J. Appl. Phys. 73 (1993), pp. 8198–8200.
[23] H. Chen, K. Chen, D.A. Drabold, and M.E. Kordesch, *Band gap engineering in amorphous AlxGa1-xN: Experiment and ab initio calculations*, App. Phys. Lett. 77 (2000), pp. 1117–1119.
[24] J.M. Khoshman and M.E. Kordesch, *Spectroscopic ellipsometry characterization of amorphous aluminum nitride and indium nitride thin films*, Phys. Status Solidi (c) 2 (2005), pp. 2821–2827.
[25] J.M. Khoshman and M.E. Kordesch, *Optical characterization of sputtered amorphous aluminum nitride thin films by spectroscopic ellipsometry*, J. Non-Cryst. Solids 351 (2005), pp. 3334–3340.
[26] F. Hajakbari, M.M. Larijani, M. Ghoranneviss, M. Aslaninejad, and A. Hojabri, *Optical properties of amorphous AlN thin films on glass and silicon substrates grown by single ion beam sputtering*, Jpn. J. of Appl. Phys. 49 (2010), pp. 095802–095807.
[27] Y. Taniyasu, M. Kasu, and T. Makimoto, *An aluminium nitride light-emitting diode with a wavelength of 210 nanometres*, Nature (London) 441 (2006), pp. 325–328.
[28] M.L. Nakarmi, K.H. Kim, K. Zhu, J.Y. Lin, and H.X. Jiang, *Transport properties of highly conductive n-type Al-rich AlxGa1–xN (x>0.7)*, Appl. Phys. Lett. 85 (2004), pp. 3769–3771.
[29] D.F. Hevia, C. Stampfl, F. Vines, and F. Illas, *Microscopic origin of n-type behavior in Si-doped AlN*, Phys. Rev. B 88 (2013), pp. 085202–085207.
[30] Y. Taniyasu, M. Kasu, and T. Makimoto, *Electrical conduction properties of n-type Si-doped AlN with high electron mobility (>100 cm2 V-1 s-1)*, Appl. Phys. Lett. 85 (2004), pp. 4672–4674.
[31] T. Ive, O. Brandt, H. Kostial, K.J. Friedland, L. Daweritz, and K.H. Ploog, *Controlled n-type doping of AlN: Si films grown on 6H-SiC (0001) by plasma-assisted molecular beam epitaxy*, Appl. Phys. Lett. 86 (2005), pp. 024106–024108.

[32] E. Monroy, J. Zenneck, G. Cherkashinin, O. Ambacher, M. Hermann, M. Stutzmann, and M. Eickhoff, *Luminescence properties of highly Si-doped AlN*, Appl. Phys. Lett. 88 (2006), pp. 071906–071908.
[33] B.N. Pantha, A. Sedhain, J. Li, J.Y. Lin, and H.X. Jiang, *Probing the relationship between structural and optical properties of Si-doped AlN*, Appl. Phys. Lett. 96 (2010), pp. 131906–131908.
[34] D. Pan, J.K. Jian, Y.F. Sun, and R. Wu, *Structure and magnetic characteristics of Si-doped AlN films*, J. Alloys and Comp. 519 (2012), pp. 41–46.
[35] W.W. Lei, D. Liu, P.W. Zhu, X.H. Chen, Q. Zhao, G.H. Wen, Q.L. Cui, and G.T. Zou, *Ferromagnetic Sc-doped AlN sixfold-symmetrical hierarchical nanostructures*, Appl. Phys. Lett. 95 (2009), pp. 162501–162503.
[36] K. Li, X. Du, Y. Yan, H. Wang, Q. Zhan, and H. Jin, *First-principles study on ferromagnetism in C-doped AlN*, Phys. Lett. A 374 (2010), pp. 3671–3675.
[37] F.Y. Ran, M. Subramanian, M. Tanemura, Y. Hayashi, and T. Hihara, *Ferromagnetism in Cu-doped AlN films*, Appl. Phys. Lett. 95 (2009), pp. 112111–112114.
[38] X.H. Ji, S.P. Lau, S.F. Yu, H.Y. Yang, T.S. Herng, and J.S. Chen, *Ferromagnetic Cu-doped AlN nanorods*, Nanotechnology 18 (2007), pp. 105601–105604.
[39] S.Y. Wu, H.X. Liu, L. Gu, R.K. Singh, L. Budd, M. van Schilfgaarde, M.R. McCartney, D.J. Smith, and N. Newman, *Synthesis, characterization and modeling of high quality ferromagnetic Cr-doped AlN thin films*, Appl. Phys. Lett. 82 (2003), pp. 3047–3049.
[40] D. Kumar, J. Antifakos, M.G. Blamire, and Z.H. Barber, *High Curie temperatures in ferromagnetic Cr-doped AlN thin films*, Appl. Phys. Lett. 84 (2004), pp. 5004–5006.
[41] Y. Endo, T. Sato, Y. Kawamura, and M. Yamamoto, *Crystal structure and magnetic properties of Cr-doped AlN films with various Cr concentrations*, Mater. Trans. 48 (2007), pp. 465–470.
[42] J. Zhang, X.Z. Li, B. Xu, and D.J. Sellmyer, *Influence of nitrogen growth pressure on the ferromagnetic properties of Cr-doped AlN thin films*, Appl. Phys. Lett. 86 (2005), pp. 212504–212506.
[43] R. Deng, K. Jiang, and D. Gall, *Optical phonon modes in Al1-xScxN*, J. Appl. Phys. 115 (2014), pp. 013506–013510.
[44] H.X. Liu, S.Y. Wu, R.K. Singh, L. Gu, D.J. Smith, N. Newman, N.R. Dilley, L. Montes, and M.B. Simmonds, *Observation of ferromagnetism above 900K in Cr–GaN and Cr–AlN*, Appl. Phys. Lett. 85 (2004), pp. 4076–4078.
[45] M.L. Nakarmi, N. Nepal, C. Ugolini, and T.M. Al Tahtamouni, J.Y. Lin, and H.X. Jiang, *Correlation between optical and electrical properties of Mg-doped AlN epilayers*, Appl. Phys. Lett. 89 (2006), pp. 152120–152122.
[46] K. Gurumurugan, H. Chen, G.R. Harp, W.M.J. Jad wisienczak, and H.J. Lozykowski, *Visible cathodoluminescence of Er-doped amorphous AlN thin films*, Appl. Phys. Lett. 74 (1999), pp. 3008–3010.
[47] W.M. Jadwisienczak, H.J. Lozykowski, F. Perjeru, H. Chen, G.R. Harp, M. Kordesch, and I.G. Brown, *Luminescence of Tb ions implanted into amorphous AlN thin films grown by sputtering*, Appl. Phys. Lett. 76 (2000), pp. 3376–3378.
[48] M.L. Caldwell, A.L. Martin, V.I. Dimitrova, P.G. Patten, M.E. Kordesch, and H.H. Richardson, *Emission properties of an amorphous AlN: Cr3+ thin-film phosphor*, Appl. Phys. Lett. 78 (2001), pp. 1246–1248.
[49] M. Maqbool, H.H. Richardson, and M.E. Kordesch, *Direct ultraviolet excitation of an amorphous AlN: Praseodymium phosphor by codoped Gd3+ cathodoluminescence*, Appl. Phys. Lett. 91 (2007), pp. 193511–193511.
[50] V. Dimitrova, P.G. Van Patten, H. Richardson, and M.E. Kordesch, *Photo-, cathodo-, and electroluminescence studies of sputter deposited AlN: Er thin films*, Appl. Surf. Sci. 175–176 (2001), pp. 480–483.
[51] F.S. Liu, Q.L. Liu, J.K. Liang, J. Luo, H. Zhang, Y. Zhang, B. Sun, and G. Rao, *Visible and infrared emissions from c-axis oriented AlN: Er films grown by magnetron sputtering*, Appl. Phys. 99 (2006), pp. 053515–053519.

[52] M.L. Caldwell, A.L. Martin, C.M. Spalding, V.I. Dimitrova, P.G. Van Patten, M.E. Kordesch, and H.H. Richardson, *Visible emission from amorphous AlN thin-film phosphors with Cu, Mn, or Cr*, J. Vac. Sci. Technol. A 19 (2001), pp. 1894–1897.
[53] M. Maqbool, I. Ahmad, G. Ali, and K. Maaz, *Energy level splitting and luminescence enhancement in AlN: Er by an external magnetic field*, Optical Mater. 46 (2015), pp. 601–604.
[54] M. Maqbool and T.R. Corn, *Optical spectroscopy and energy transfer in amorphous AlN-doped erbium and ytterbium ions for applications in laser cavities*, Opt. Lett. 35 (2010), pp. 3117–3119.
[55] P. Ordejón, E. Artacho, and J.M. Soler, *Self-consistent order-N density-functional calculations for very large systems*, Phys. Rev. B 53 (1996), pp. 10441–10444.
[56] M. Durandurdu, *Pressure-induced phase transition in AlN: An ab initio molecular dynamics study*, J. Alloys and Comp. 480 (2009), pp. 917–921.
[57] M. Durandurdu, *Uncovering nanoclusters in amorphous aln: An Ab initio study*, J. Am. Ceram. Soc. 98 (2015), pp. 1095–1098.
[58] N. Troullier and J.M. Martins, *Efficient pseudopotentials for plane-wave calculations*, Phys. Rev. B 43 (1991), pp. 1993–2006.
[59] A.D. Becke, *Density-functional exchange-energy approximation with correct asymptotic behavior*, Phys. Rev. A 38 (1988), pp. 3098–3100.
[60] C. Lee, W. Yang, and R.G. Parr, *Development of the Colle-Salvetti correlation-energy formula into a functional of the electron density*, Phys. Rev. B 37 (1998), pp. 785–789.
[61] M. Parrinello and A. Rahman, *Polymorphic transitions in single crystals: A new molecular dynamics method*, J. Appl. Phys. 52 (1981), pp. 7182–7190.
[62] K. Momma and F. Izumi, *VESTA 3 for three-dimensional visualization of crystal, volumetric and morphology data*, J. Appl. Crystall. 44 (2011), pp. 1272–1276.
[63] J. Musil, M. Šašek, P. Zeman, R. Čerstvý, D. Heřman, J.G. Han, and V. Šatava, *Properties of magnetron sputtered Al–Si–N thin films with a low and high Si content*, Surf. Coat. Technol. 202 (2008), pp. 3485–3493.
[64] A. Pélisson-Schecker, H.J. Hug, and J. Patscheider, *Morphology, microstructure evolution and optical properties of Al–Si–N nanocomposite coatings*, Surf. Coat. Technol. 257 (2014), pp. 114–120.
[65] H. Liu, W. Tang, D. Hui, L. Hei, and F. Lu, *Characterization of (Al, Si) N films deposited by balanced magnetron sputtering*, Thin Solid Films 517 (2009), pp. 5988–5993.
[66] D. Pan, J.K. Jian, Y.F. Sun, and R. Wu, *Structure and magnetic characteristics of Si-doped AlN films*, J. Alloys Compd. 519 (2012), pp. 41–46.
[67] K. Jarolimek, R.A. De Groot, G.A. De Wijs, and M. Zeman, *Atomistic models of hydrogenated amorphous silicon nitride from first principles*, Phys. Rev. B 82 (2010), pp. 205201–205209.
[68] L. Giacomazzi and P. Umari, *First-principles investigation of electronic, structural, and vibrational properties of a-Si3N4*, Phys. Rev. B 80 (2009), pp. 144201–144212.
[69] K. Chen and D.A. Drabold, *First principles molecular dynamics study of amorphous AlxGa1-xN alloys*, J. App. Phys. 91 (2002), pp. 9743–9751.
[70] B. Cai and D.A. Drabold, *Properties of amorphous GaN from first-principles simulations*, Phys. Rev. B 84 (2011), pp. 075216–075221.
[71] B. Cai and D.A. Drabold, *Ab initio models of amorphous InN*, Phys. Rev. B 79 (2009), pp. 195204–195207.
[72] J. Ziman, *Models of disorder, the theoretical physics of homogeneously disordered systems*, Cambridge University Press, London, 1979.
[73] Y. Li and D.A. Drabold, *Electronic signatures of topological disorder in amorphous grapheme*, IET Circuits, Devices & Systems 9 (2014), pp. 13–18.